



OPEN ACCESS

EDITED BY

Regiane R. Santos,
Schothorst Feed Research, Netherlands

REVIEWED BY

Faizul Hassan,
Cholistan University of Veterinary and Animal
Sciences, Pakistan
Jihu Zhang,
Tarim University, China

*CORRESPONDENCE

Weina Cao
✉ 849989054@qq.com
Changrong Ge
✉ gcrzal@126.com

†These authors have contributed equally to
this work

RECEIVED 27 October 2025

REVISED 26 December 2025

ACCEPTED 29 December 2025

PUBLISHED 29 January 2026

CITATION

Liu M, Ruan J, Yang Y, Li M, Gu Z, Ge C and
Cao W (2026) Effects of guanidinoacetic acid
on gene expression in adipose tissue of broiler
chickens: a differential expression analysis
based on small RNA sequencing.
Front. Vet. Sci. 12:1732976.
doi: 10.3389/fvets.2025.1732976

COPYRIGHT

© 2026 Liu, Ruan, Yang, Li, Gu, Ge and Cao.
This is an open-access article distributed
under the terms of the [Creative Commons
Attribution License \(CC BY\)](#). The use,
distribution or reproduction in other forums is
permitted, provided the original author(s) and
the copyright owner(s) are credited and that
the original publication in this journal is cited,
in accordance with accepted academic
practice. No use, distribution or reproduction
is permitted which does not comply with
these terms.

Effects of guanidinoacetic acid on gene expression in adipose tissue of broiler chickens: a differential expression analysis based on small RNA sequencing

Mengqian Liu^{1,2,3†}, Jinrui Ruan^{1†}, Yu Yang^{1†}, Mengyuan Li¹,
Zifu Gu¹, Changrong Ge^{1,4*} and Weina Cao^{1,4*}

¹College of Animal Science and Technology, Yunnan Agricultural University, Kunming, China, ²Key Laboratory of Feed Biotechnology, Ministry of Agriculture and Rural Affairs, Institute of Feed Research, Chinese Academy of Agricultural Sciences, Beijing, China, ³College of Animal Science and Technology, Gansu Agricultural University, Gansu, China, ⁴Yunnan Provincial Key Laboratory of Animal Nutrition and Feed, Yunnan Agricultural University, Kunming, China

This study aims to elucidate the mechanism by which guanidinoacetic acid (GAA) reduces abdominal fat deposition in broilers, focusing on the regulatory role of microRNAs (miRNAs). Excessive fat accumulation in the abdomen is a common issue in meat-type chickens as it reduces feed efficiency and compromises meat quality. By performing small RNA (sRNA) sequencing and analysis on broilers from GAA-treated and control groups, a total of 46 differentially expressed miRNAs were identified. Gene Ontology (GO) and Kyoto Encyclopedia of Genes and Genomes (KEGG) enrichment analyses indicated that these miRNAs were significantly enriched in pathways related to lipid metabolism. Further investigation revealed that GAA likely reduces fat deposition and promotes lipid oxidation by up-regulating gga-miR-103-3p and gga-miR-107-3p, thereby inhibiting their target genes, stearoyl-CoA desaturase (SCD) and transmembrane protein 35B (TMEM35B). These findings provide a theoretical foundation for the application of GAA to improve growth performance and meat quality in broilers.

KEYWORDS

adipose, broiler, fat deposition, guanidinoacetic acid, microRNA, transcriptome

1 Introduction

New intensive farming methods and selective breeding have improved the growth rates and feed conversion efficiencies of broiler chickens (1, 2). Nevertheless, rapid growth in some breeds is associated with increased deposition of fat, particularly in the abdominal and subcutaneous regions (3). A surplus of fat damages meat quality, raises feed costs, impacts the environment and harms consumer health (4–6). Abdominal adipocytes exhibit higher metabolic activity and greater lipogenic potential (7, 8). Therefore, understanding the molecular pathways responsible for abdominal fat accumulation is crucial.

Guanidinoacetic acid (GAA) is the primary biosynthetic precursor of creatine in vertebrates (9, 10). Creatine is nitrogenous organic acid vital for supplying energy for fast growth and development of muscle tissue via the creatine and phosphocreatine pathway (11–13). Studies show that dietary GAA elevates the concentration of creatine in animal

tissues to improve performance, feed conversion efficiency, and enhance antioxidant capacity (12, 14). GAA improves the efficacy of utilizing phosphocreatine-derived energy, a speedy source of ATP for muscle and liver tissues, and also aids its synthesis (11, 15–17). Furthermore, studies indicate that creatine, targeting the PI3K signaling pathway, can block the differentiation of adipocyte at the early stage (18). Thermogenic adipocytes may use creatine to activate futile cycles, contributing to the regulation of energy metabolism.

Molecules like stearoyl-CoA desaturase 1 (SCD1) and transmembrane protein (TMEM) family members (e.g., TMEM35B) are already known to modulate lipid synthesis, adipocyte differentiation and energy metabolism. SCD1 acts as a rate-limiting enzyme for monounsaturated fatty acid production and modulates adipocyte lipid composition and metabolic state directly (19, 20). MicroRNA-103/107 (miR-103/107) family also is critical to metabolism because it targets the transcription factor C/EBP α to inhibit adipogenesis and enhances insulin sensitivity (21). It is, however, unclear whether and how the feed additive GAA influences abdominal fat deposition in poultry through these pathways. Studies on the fat-reducing effects of GAA have focused on growth performance, slaughter traits, and a limited set of serum biochemical markers (22, 23), but have not employed systematic transcriptomic or post-transcriptional network analyses. Thus, elucidating how GAA regulates key molecules such as SCD1, TMEM proteins, and miR-103/107 may provide a strategy to mitigate abdominal fat deposition.

Studies on GAA as a poultry feed additive have focused primarily on production performance and meat quality (24–26). In contrast, its specific impact on abdominal fat deposition remains poorly understood, with only limited research, such as the study by Wu et al. (23), having addressed this aspect. Our previous study showed that dietary supplementation with 1.2 g/kg GAA significantly reduced abdominal fat percentage and adipocyte size in Cobb broilers. While both 1.2 and 3.6 g/kg GAA improved growth performance, the lower dose (1.2 g/kg) proved superior for enhancing breast yield, thigh yield, and meat quality (27). Therefore, the 1.2 g/kg dose was selected for further investigation based on its optimal effects on carcass yield and meat quality. However, the mechanism underlying its fat-reducing action remained unknown. To address this, we performed an integrated analysis of microRNA (miRNA) and mRNA expression using bioinformatics, constructing a regulatory network of miRNAs involved in abdominal fat development in Cobb broilers. This work expands the repertoire of known avian miRNAs in abdominal adipose tissue and offers new insights into miRNA-mediated regulation of fat deposition.

2 Materials and methods

2.1 Ethics statement

All experimental procedures and operations received approval from the Life Sciences Ethics Committee at Yunnan Agricultural University (Approval ID: 202203094). The research was carried out in compliance with regional laws and institutional guidelines.

2.2 Collection of abdominal fat tissue from experimental chickens

Hunan Shuncheng Industrial Co., Ltd. supplied one-day-old Cobb chicks, which were then accommodated in stacked cages. Controlled conditions as to temperature, humidity and air flow were maintained in these cages. The diet plan consisted of corn-soybean meal pellets while the control group got the feed. The nutritional composition and makeup of the base diet utilized during the preliminary phase of the study are illustrated in Table 1. At the same time, Table 2 outlines the nutritional characteristics and composition of the base diet implemented in the later phase. All experimental groups received an isocaloric basal diet. The experimental group (GAA group) was supplemented with 1.2 g/kg of guanidinoacetic acid by replacing an equal amount of carrier to maintain identical total caloric content with the control group. Moreover, in the GAA group, we incorporated another 1.2 g/kg dose of guanidinoacetic acid in the basal diet, which was provided to the chickens until they reached 42 days of age. The experiment incorporated solely male broiler chicks. At the end of the experiment, all chickens were humanely euthanized by cervical dislocation. Tissues of abdominal fat of three chickens from each group were collected. The tissues were quickly frozen with liquid nitrogen and stored at -80°C for analysis.

2.3 Sequencing of small RNA (sRNA)

2.3.1 RNA isolation, sRNA library construction, and sequencing

The Trizol reagent was used for RNA extraction. Agarose gel electrophoresis was used to check RNA integrity and contamination. Nanodrop instrument was used to check RNA purity. The quantity of the RNA was quantified using Qubit and the quality of RNA was assessed using the Agilent 2100 system. The sRNA Sample Pre Kit was used to construct the sRNA library from abdominal fat tissue following the assessment of quality. This technique gained its basis through the exclusive structures at the 3' and 5' end of sRNA. Onto these ends are attached a complete phosphate group at the 5' end and a hydroxyl group at the 3' end. The process started with the extraction of total RNA. After that, adapters were ligated to both ends of the sRNA and reverse transcribed to cDNA. After the PCR amplification phase, the target DNA fragments were separated using PAGE gel electrophoresis. The gel was then excised to obtain the cDNA library. Once the library construction was completed, an initial quantification was performed using a Qubit 2.0 device. The library was diluted to a concentration of 1 ng/ μl . Following this, the size of the insert was assessed with an Agilent 2100 system (Agilent Technologies, CA, United States). Finally, the effective concentration was determined via RT-qPCR, ensuring that a satisfactory effective concentration exceeded 2 nM. Libraries meeting the quality standards were subsequently sequenced by Beijing Novogene Technology Co., Ltd. employing the Illumina SE50 technique.

TABLE 1 Composition of the basal diet (%).

Ingredients	Brooding period	Breeding period
Corn	61.20	60.90
Soybean meal	30.16	25.22
Fish meal	3.60	0.00
Wheat bran	0.00	10.00
Soybean oil	1.10	0.00
CaHPO ₄	1.50	1.50
Limestone	0.70	0.60
Zeolite powder	0.41	0.46
L-Met	0.08	0.07
NaCl	0.25	0.25
Premix	1.00	1.00

The premix for each kilogram of the diet provides the following nutrients: vitamin A (VA) 15 000 U, VD₃ 3300 U, VE 62.5 mg, VK 3.6 mg, VB₁ 3.0 mg, VB₂ 9.0 mg, VB₆ 6.0 mg, VB₁₂ 0.03 mg, folic acid 60 mg, niacin 60 mg, pantothenic acid 18 mg, Biotin 0.36 mg, choline chloride 600 mg, Se 0.15 mg, I 0.35 mg, Cu 12 mg, Mn 60 mg, Fe 80 mg, Zn 75 mg, and other additives such as antibacterial growth promoting agents and antioxidants.

TABLE 2 Nutrient levels of the basal rations.

Nutrient components	Brooding period	Breeding period
Metabolizable energy/(MJ/kg)	12.13	11.63
Crude protein (%)	19.30	15.50
Lysine (%)	0.98	0.79
Methionine (%)	0.08	0.07
Calcium (%)	0.85	0.80
Available phosphorus (%)	0.37	0.37

The metabolizable energy was calculated, while the remaining portion was quantified.

2.3.2 Quality control of sRNA sequencing and reference genome alignment

Raw sequencing reads underwent processing to evaluate sequencing quality, determine the length distribution of sRNA reads, and eliminate sequences exhibiting more than 10% N content, low-quality sequences, those containing 5' adapters, sequences lacking 3' adapters or insertion fragments, as well as sequences with polyA/T/G/C. Clean reads within the range of 18–35 nt were subsequently employed in the ensuing analyses.

The Bowtie (v0.12.9) software was used to align length-filtered clean reads with the chicken genome, facilitating the annotation of various RNA types, including rRNA, tRNA, snRNA, snoRNA, and repetitive sequences. Subsequently, the remaining sequences were compared with the chicken miRBase database to identify known miRNAs. At the same time, the unannotated sequences were aligned with the chicken genome sequence to uncover potential novel miRNAs. To predict the hairpin structures and

folding energies of these sequences, MiREvo (v1.1) and mirdeep2 (v2.0.0.5) were utilized. Only sequences that exhibited stem-loop hairpin structures were considered as potential novel miRNAs. Ultimately, we retained high-confidence candidate miRNAs that had a miRDeep2 composite score >4 and were supported by all structural and evolutionary filters in the miREvo analysis.

2.3.3 Analysis of differential miRNA expression

For the differential expression analysis of miRNAs, the expression levels of both known and novel miRNAs were statistically evaluated, and normalization was performed using the Transcripts Per Million (TPM) method. The normalized expression values were calculated utilizing the formula: (read count × 1,000,000)/total miRNA read count in the library. Differentially expressed miRNAs were identified through the DESeq2 (v1.20.0) software, which conducts pairwise sample analysis based on a negative binomial distribution, applying a threshold of P -value < 0.05 and $|\log_2(\text{fold change})| > 1$.

2.3.4 Differentially expressed miRNA target gene prediction, gene ontology (GO) and Kyoto encyclopedia of genes and genomes (KEGG) enrichment analysis

The prediction of target genes for differentially expressed miRNAs was achieved using both miRanda (v2.0.0.8) and RNAhybrid (v2.1.2) software, with the intersection of results taken into consideration. To investigate the functional characteristics of target genes, we performed GO enrichment analysis using GOSeq/topGO (Release 2.12). Meanwhile, pathway enrichment analysis was conducted with KOBAS (v2.0) based on the KEGG database to identify significantly associated pathways. In the analysis, the Benjamini–Hochberg (BH) method was applied for multiple testing correction of P -values in enrichment analysis. Pathways or functional terms with adjusted P -values < 0.05 were considered significantly enriched.

2.3.5 sRNA sequencing analysis

This study employed standardized statistical methods and software for data analysis rigor for its data analysis. Following the quality assessment of raw sequencing data, the sequences containing >10% N bases, low-quality reads, adapter-contaminated reads, and polyA/T/G/C sequences were filtered out. Meanwhile, the clean reads of lengths 18–35 nt were reserved for the further analysis. The sequences were aligned to the chicken reference genome using Bowtie (v0.12.9), followed by comprehensive RNA annotation. Known miRNAs were identified by aligning with the miRBase database, while novel miRNAs were predicted using both MiREvo (v1.1) and mirdeep2 (v2.0.0.5) software, with only sequences exhibiting typical stem-loop structures being retained as candidates.

miRNA expression levels were normalized using transcripts per million (TPM) method. Differential expression analysis was performed using DESeq2 (v1.20.0) software, with screening criteria set at adjusted P -value < 0.05 and $|\log_2(\text{fold change})| > 1$.

For the prediction of target genes of differentially expressed miRNAs, the results from both miRanda (v2.0.0.8) and RNAhybrid (v2.1.2) software were integrated, with their intersection taken as the final predicted target genes. Subsequently, GOSeq/topGO (Release 2.12) was employed for GO enrichment analysis, and KOBAS (v2.0) was used for KEGG pathway enrichment analysis. All enrichment analysis results were adjusted for *P*-values using the Benjamini–Hochberg (BH) method, with an adjusted *P*-value <0.05 considered statistically significant.

2.4 Transcriptome sequencing

2.4.1 Total RNA extraction and transcriptome sequencing of abdominal fat tissue

In terms of transcriptome sequencing, total RNA was extracted from abdominal fat tissue using TRIzol Reagent. The concentration and purity of RNA were assessed via a NanoDrop 2000 spectrophotometer, and RNA integrity was precisely evaluated using the RNA Nano 6000 detection kit from the Agilent Bioanalyzer 2100. After confirming the quality of the RNA, a cDNA library was generated, followed by sequencing on the Illumina NovaSeq 6000 platform in PE150 configuration. The sequencing was conducted by Beijing Novogene Technology Co., Ltd. Clean data, effectively filtered to remove sequences with adapters, poly-*N* sequences, and low-quality reads (wherein reads displayed more than 10% *N* or where over 50% of the bases had a quality score of $Q \leq 10$), were acquired. The resulting clean reads were then aligned to the reference genome utilizing the HISAT2 (v2.0.5) software. Following this, StringTie (v1.3.3b) was used to assemble and reconstruct the aligned reads. Ultimately, gene expression levels were computed through the Fragments Per Kilobase of transcript per Million mapped reads (FPKM) method.

2.4.2 Differential expression gene screening

Based on the alignment results, raw read counts mapped to each gene were quantified using the featureCounts (v1.5.0p3). The DESeq2 (v1.20.0) package was used for the differential expression analysis of the data with raw count matrix as input. The first step of the software is that it assesses the raw count data by estimating size factors to normalize for library size. The second step is fitting a negative binomial distribution model, which will estimate dispersion at the gene level. The Benjamini and Hochberg method was applied to control the false discovery rate, yielding adjusted *P*-values. The criteria of $|\log_2\text{FC}| > 1$ and $P \leq 0.05$ were used to filter differentially expressed genes (DEGs), and visualizations of the differences between the two groups were created using heatmaps and volcano plots.

2.4.3 Differential expression genes GO and KEGG pathway enrichment analysis

The analysis of GO enrichment for DEGs was ultimately conducted using the clusterProfiler (v3.8.1) package. The Wallenius non-central hypergeometric distribution was used in

the assessment to correct for gene length bias in DEGs. Alongside clusterProfiler (v3.8.1), the KOBAS (v2.0) database facilitated the KEGG enrichment analysis of DEGs.

2.4.4 Transcriptome sequencing analysis

This study employed standardized procedures for transcriptome data analysis. Quality-controlled sequencing data were aligned to the reference genome using HISAT2 (v2.0.5) and assembled via StringTie (v1.3.3b). Gene expression levels were quantified as FPKM values. Differential expression analysis was performed based on the raw count matrix generated by featureCounts (v1.5.0p3) using DESeq2 (v1.20.0), which executed library size normalization, negative binomial model fitting, and dispersion estimation. The Benjamini–Hochberg method was applied for *P*-value adjustment to control the false discovery rate. The screening criteria for DEGs were $|\log_2\text{FC}| > 1$ and adjusted $P \leq 0.05$. GO enrichment analysis was performed using clusterProfiler (v3.8.1) software with correction for gene length bias; KEGG pathway enrichment analysis was conducted using the KOBAS (v2.0) database, and the results were visualized through heatmaps and volcano plots.

2.5 RT-qPCR verification of differential expression mRNA and miRNA

To confirm the differentially expressed mRNA and miRNA, RT-qPCR techniques were applied. Total RNA was extracted from adipose tissue samples employing TRIzol. The identified differentially expressed miRNAs were reliable, we selected five miRNAs for RT-qPCR validation alongside six DEGs. The primers for mRNA were designed utilizing Prime 5.0 software (Table 3), whereas those for miRNA were developed through miRprimer2 software (Table 4). The synthesis of these primers was conducted by Kunming Qingke Biotechnology Co., Ltd. For the quantification of relative expression levels, GAPDH and U6 served as internal controls for DEMs and DEGs, respectively.

The mRNA quantitative fluorescence reaction total volume was set to 20 μl . The solution had 12.5 μl of (2 \times) TB Green Premix Ex Taq II (Tli RNase H Plus), 1 μl each of upstream and downstream primers, 2 μl of cDNA and 8.5 μl of double-distilled water (ddH₂O). The initial step was denaturation at five degrees Celsius for 5 min after forty cycles. Every cycle consists of a denaturation step at 95 °C for 15 s and heating at 60 °C for 45 s.

Conversely, the quantitative fluorescence reaction system for miRNA was established with an overall volume of 25 μl . This configuration included 12.5 μl of 2 \times TB Green Premix Taq II, 0.5 μl of a primer specific to miRNA, 0.5 μl of the mR3' Primer; 2.5 μl of cDNA, and 9 μl of RNase-free ddH₂O. The reaction protocol began with 15 s of pre-denaturation at 95 °C, followed by 5 s of denaturation at 95 °C, and 20 seconds of annealing at 60 °C. The said sequence was similar to that of 40 cycles. To ensure that the results were accurate, three biological replicates were done for each sample.

TABLE 3 Primer sequences of mRNAs used for RT-qPCR.

Accession number	Gene name	Primer sequence (5/3')	Length (bp)
NM_204305.1	GAPDH	F: CTGGGGCTCATCTGAAGGGT	308
		R: GGACGCTGGGATGATGTTCT	
NM_204272.2	RPL39L	F: ATGTCGTCTCACAAGACCTTCAAGA	263
		R: CAGCACTACAGAAGGAATGACATGA	
NM_001012545.2	GPM6B	F: TTTTCCTCACCTACGTGCTTGG	138
		R: CTCCTGGAACCGTCATGTTTATC	
XM_046901266.1	MORN3	F: GGACGATGTTCTACCCACGC	103
		R: TCATAGGTGGACCCGCTCC	
NM_001031305.2	SLC9A9	F: TATGGGATCCTCTTATGCAGTTGTC	144
		R: ATACCTGTGAGACCAGCAGCTTC	
NM_001199595.2	PHLDA2	F: CAAGGAGATTGACTTTCGGTGC	85
		R: CCTCTTGTCTGGAAGTCGATG	
XM_040696392.2	CTHRC1	F: ATAGCGGAATGTACGTTCAAAAGA	249
		R: GTTGATCCCTTCACACAGACCTT	

TABLE 4 Primer sequences of miRNAs used for the stem-loop RT-qPCR.

Primer name	Primer sequence(5/3')	Length (bp)
U6	F: CTCGCTTCGGCAGCACACA	94
	R: AACGCTTCACGAATTTGCGT	
gga-miR-455-3p	Loop: CTCAACTGGTGTCTGGAGTCGGCAATTCAGTTGAGGTGTATAT	66
	F: ACACTCCAGCTGGGTGCAGTCCATGGGCAT	
	R: TGGTGTCTGGAGTCG	
gga-miR-183	Loop: CTCAACTGGTGTCTGGAGTCGGCAATTCAGTTGAGCAGTGAAT	67
	F: ACACTCCAGCTGGGTATGGCACTGGTAGAAT	
	R: TGGTGTCTGGAGTCG	
gga-miR-17-5p	Loop: CTCAACTGGTGTCTGGAGTCGGCAATTCAGTTGAGACTACCTG	68
	F: ACACTCCAGCTGGCAAAGTGCTTACAGTGCA	
	R: TGGTGTCTGGAGTCG	
gga-miR-9-5p	Loop: CTCAACTGGTGTCTGGAGTCGGCAATTCAGTTGAGTCATACAG	67
	F: ACACTCCAGCTGGGTCTTTGGTTATCTAGCT	
	R: TGGTGTCTGGAGTCG	
gga-miR-129-5p	Loop: CTCAACTGGTGTCTGGAGTCGGCAATTCAGTTGAGGCAAGCCC	65
	F: ACACTCCAGCTGGGCTTTTTCGGTCTGG	
	R: TGGTGTCTGGAGTCG	

3 Results

3.1 Quality control of sRNA sequencing data

The quality assessment of the six samples confirmed their suitability for constructing sRNA libraries and further experimentation. After sequencing, the raw data went through quality control performed by custom scripts developed in Perl

and Python. The initial read counts spanned from 13,390,828 to 15,505,114. After quality control, the valid read counts ranged from 13,032,440 to 15,515,785. All the samples displayed Q20 scores more than 98% while the Q30 scores were above 96%. The GC content for each sample was between 48.90 and 53.22%. The acquisition of high-quality sequencing data, coupled with consistent GC content, indicates that the sequencing quality is adequate for further analysis. Detailed quality control metrics for each sample can be found in Table 5.

TABLE 5 Summary of the quality of sequencing data output.

Sample	Total reads	Clean reads	Q20	Q30	GC content
CK_1	13,390,828	13,032,440 (97.32%)	98.96%	96.28%	50.47%
CK_2	14,903,068	14,607,373 (98.02%)	98.97%	96.17%	53.22%
CK_3	13,935,469	13,675,100 (98.13%)	99.06%	96.81%	49.28%
GAA_1	15,249,332	14,994,452 (98.33%)	99.06%	96.63%	49.87%
GAA_2	15,788,637	15,515,785 (98.27%)	99.57%	98.27%	48.90%
GAA_3	15,505,114	15,288,859 (98.61%)	99.56%	98.07%	50.92%

Sample is the sample id; reads is statistical raw sequence data; bases were the number of sequencing sequences multiplied by the length of sequencing sequences and converted to G; Error rate is the sequencing error rate; Q20 was the percentage of bases with Phred value greater than 20 in the total base; Q30 is the percentage of bases with Phred value greater than 30 in the total base; GC content is the percentage of the total number of bases G and C combined to calculate the total number of bases.

3.2 Length distribution of sRNAs

With high-throughput sequencing technology, we can sequence and quantitatively assess the expression of all the sRNA families present in the sample. Therefore, it is possible to analyze upstream of miRNAs, siRNAs, piRNAs and other non-coding RNAs and their target sequences. The clean reads recovered led to the selection of sRNAs with a size ranging from 18 to 35 nucleotides (Table 6). The sequenced sRNAs ranged between 20 and 24 nucleotides (Figure 1), which were Dicer products. The sRNAs show a peak at 22 nucleotides, which is also the length class for animal miRNAs.

3.3 Genome alignment of sRNAs

Using Bowtie (v0.12.9), the filtered sRNAs were subjected to the complete sequence alignment to a reference genome. As per the results, a significantly high proportion of clean reads were effectively mapped on the reference genome. The control group had an observed value of 88.27%. By contrast, the mapping rate for the GAA group was slightly lower (86.33%). The average percentages of reads aligning in the same orientation to the reference sequence were 56.64% and 50.70%, respectively, while those aligning in the opposite direction averaged 31.63% and 35.62%. Table 7 summarizes the complete information regarding the alignment of samples.

3.4 Screening of differentially expressed miRNAs and RT-qPCR validation

In order to significantly compare the specimens, the expression levels of the known miRNAs and the newly identified miRNAs in each specimen were measured. To ensure consistency and reliability in the analysis, these expression levels were normalized using a metric known as transcripts per million (TPM). Pairwise analysis was performed using DESeq2 (v1.20.0) with negative binomial distribution, as shown in the volcano plot in Figure 2A. According to the volcano plot, the expression level of 46 miRNAs is significantly different between the control groups and GAA. Fifteen miRNAs showed upregulation while 31 miRNAs showed

downregulation. The validity of these differentially expressed miRNAs requires further investigation.

The expression levels of miRNAs were influenced by GAA. A hierarchical clustering analysis on differentially expressed miRNAs across the six samples (Figure 2B) classified the six samples into two major branches, indicating high consistency among the samples and hence strength of the experimental design and analysis. Among the various miRNAs that show differential expression, a few have been identified as significant to fat deposition, particularly gga-miR-455-3p and gga-miR-425-5p. A subset of five differentially expressed miRNAs was randomly chosen for validation via reverse transcription quantitative polymerase chain reaction (RT-qPCR), with results that closely matched those obtained from sRNA sequencing (Figure 2C). This concordance emphasizes the consistency and reliability of the sRNA sequencing data, thereby affirming its appropriateness for further analytical endeavors.

3.5 Prediction and bioinformatics analysis of miRNA target genes with differential expression

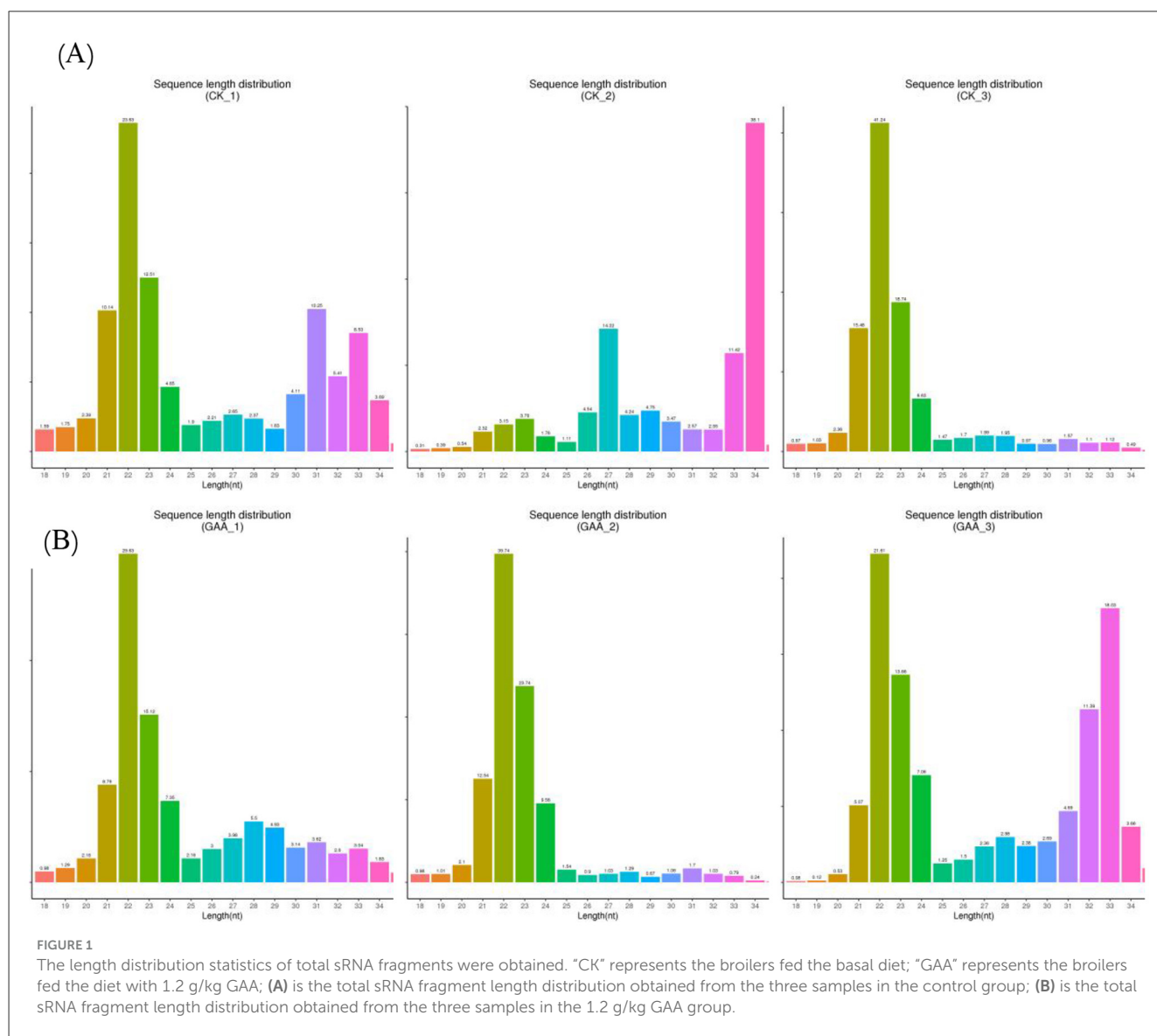
In the following section, titled Target Gene Prediction for Differentially Expressed miRNAs and Bioinformatics Analysis, the prediction of target genes for the identified differentially expressed miRNAs was performed by analyzing their interactions with the help of miRanda (v2.0.0.8) and RNAhybrid (v2.1.2) software. This analysis enabled the discovery of target genes linked to the miRNAs that were expressed differently. The results indicated that one miRNA has the potential to control numerous genes, while on the other hand, a singular gene can be influenced by multiple miRNAs. Interestingly, the miRNAs predicted to have the most significant regulatory influence on target genes were gga-miR-1625-5p (which regulates 251 genes), gga-miR-7455-3p (influencing 196 genes), gga-miR-107-3p (affecting 175 genes), gga-miR-103-3p (impacting 161 genes), gga-miR-12283-3p (regulating 111 genes), gga-miR-2131-5p (which regulates 91 genes), gga-miR-3528 (overseeing 83 genes), gga-miR-455-3p (controlling 77 genes), and gga-miR-130b-5p (regulating 63 genes).

Furthermore, enrichment analyses were conducted utilizing GO and the KEGG on gene sets linked to the differentially expressed miRNAs (see Figures 3A, B). The findings from the

TABLE 6 The number and types of sRNA after length screening.

Sample	Total reads	Total bases (bp)	Uniq reads	Uniq bases (bp)
CK_1	11,972,029	308,127,458	523,612	13,007,621
CK_2	14,223,118	429,836,924	479,679	12,434,120
CK_3	13,108,789	301,296,434	403,603	9,710,912
GAA_1	14,429,382	355,733,707	921,892	23,609,083
GAA_2	15,028,789	344,406,103	350,208	8,305,202
GAA_3	14,746,635	399,498,360	308,054	8,468,730

Sample is the sample id; total reads is the total number of sRNAs; total bases (bp) is the total length of the sRNA; uniq reads is the type of sRNA; uniq bases (bp) are the total length of each sRNA.



GO enrichment analysis indicated that the target genes in the GAA group showed a marked enrichment in processes related to catalytic activities, cellular nuclear functions, and peptidase activity when compared to the control group. Similarly, the KEGG enrichment assay indicated that the target genes in the GAA group were significantly enriched in metabolic processes, regulation of

actin cytoskeleton, endocytosis, lysosome functions, apoptosis, and protein processing in the endoplasmic reticulum.

Lipid metabolic pathways were highly enriched in genes with member functions. Lipid synthesis (lipogenesis) and lipid breakdown (lipolysis) are the main metabolic processes. The synthesis and proper folding of enzymes and membrane proteins

TABLE 7 Comparisons with reference sequences.

Sample	Total sRNA	Mapped sRNA	+ Mapped sRNA	– Mapped sRNA
CK_1	11,972,029 (100.00%)	1,0476,888 (87.51%)	6,161,716 (51.47%)	4,315,172 (36.04%)
CK_2	14,223,118 (100.00%)	12,029,114 (84.57%)	10,995,417 (77.31%)	1,033,697 (7.27%)
CK_3	13,108,789 (100.00%)	12,154,329 (92.72%)	5,393,263 (41.14%)	6,761,066 (51.58%)
GAA_1	14,429,382 (100.00%)	11,599,574 (80.39%)	6,959,149 (48.23%)	4,640,425 (32.16%)
GAA_2	15,028,789 (100.00%)	14,148,598 (94.14%)	6,889,187 (45.84%)	7,259,411 (48.30%)
GAA_3	14,746,635 (100.00%)	12,453,480 (84.45%)	8,558,301 (58.04%)	3,895,179 (26.41%)

Sample is the sample id; total sRNA, clean reads of each sample obtained after length screening; mapped sRNA, the number and percentage of clean reads mapped to the reference sequence in the sample; +mapped sRNA, the number and percentage of reads in the clean reads of the sample that are mapped to the same direction of the reference sequence; –mapped sRNA, the number and percentage of reads in the clean reads of the sample that are mapped to the chain in the opposite direction of the reference sequence.

that are necessary for lipid synthesis requires protein processing in the endoplasmic reticulum. Moreover, the actin cytoskeleton was regulated, which is important to adipocyte differentiation and lipid droplet dynamics, playing a pivotal role in adipose tissue expansion. Lipid mobilization and turnover pathways were also significantly enriched. Functions of lysosome directly take part in lipid degradation from lipophagy. Endocytosis can modulate lipid signaling and uptake by regulating membrane receptors and transporters. Moreover, apoptosis is involved in adipose tissue remodeling and may influence overall lipid homeostasis indirectly. Together, these enriched pathways suggest that GAA treatment may modulate the molecular machinery controlling fat deposition and degradation.

3.6 Transcriptome analysis

The expression levels of known and novel mRNAs were quantified and normalized across each sample using Transcripts Per Million (TPM) in the Transcriptome Analysis section. Using DESeq2 (version 1.20.0) and the negative binomial distribution, we performed sample pairwise analysis which resulted in a volcano plot shown in Figure 4A. The volcano plot reveals that 861 mRNAs significantly differed in expression between the GAA group and the control group, with 392 mRNAs upregulated and 469 mRNAs downregulated. To investigate the relationship of GAA with the mRNA expression levels, we performed a hierarchical clustering analysis of differentially expressed mRNAs from the six samples (Figure 4B). This analysis effectively separated the six samples into two main branches, which indicated strong sample consistency and a sound study design. Fat deposition-related mRNAs were both RPL39L and MORN3 among differentially expressed mRNAs. Four randomly selected differentially expressed mRNAs were validated using RT-qPCR, and the results were consistent with transcriptome sequencing data (Figure 4C), which further verified the reproducibility and reliability of the transcriptome sequencing data.

Therefore, enrichment analyses for GO and KEGG were performed for the DEGs (Figures 5A, B). According to the GO enrichment assessment, compared to control genes, GAA genes mainly have extracellular matrix-related functions.

The KEGG enrichment analysis on DEGs reveals that, compared to control, the GAA group shows primary enrichment

for several categories. These included CAMs, focal adhesion, synthesis of steroid hormones, phagosome dynamics, biosynthesis of mucin-type O-glycans and synthesis of pantothenic acid and coenzyme A. In addition, the analysis analyzed the AGE-RAGE signaling pathway with respect to complications arising from diabetes.

Focal adhesions and cell adhesion molecules (CAMs) play a role in adipocyte differentiation, lipid droplet formation, and overall adipose tissue expansion and remodeling. The AGE-RAGE signaling pathway acts as a crucial pro-inflammatory and profibrotic pathway in diabetic complications. The phenomenon of enrichment suggests a potential mechanism through which GAA may impact inflammatory, fibrotic, and insulin-sensitive features of adipose tissue, leading to a concurrent regulation of lipid storage capacity (deposition) and metabolic turnover. The biosynthesis of steroid hormones, which act as potent regulators (e.g. glucocorticoids and sex hormones), is directly relevant.

3.7 Analysis of differential expression miRNA and mRNA regulatory networks

To generate a network diagram using Cytoscape, we collected gene targets of differentially expressed miRNAs with results of DEGs in our regulatory network analysis of expression differentially expressed miRNAs and mRNAs. Within the networks of the GAA group and the control group (Figure 6), 25 miRNAs were linked to 86 DEGs, thereby building a complex network. This includes miRNAs such as gga-miR-9b-3p, gga-miR-129-5p, gga-miR-7455-3p, gga-miR-217-5p, gga-miR-9-5p, gga-miR-17-5p, gga-miR-20b-5p, gga-miR-425-5p, gga-miR-183, gga-miR-1625-5p, gga-miR-103-3p, gga-miR-107-3p, gga-miR-2131-5p, gga-miR-130b-5p, gga-miR-12283-3p, gga-miR-3536, gga-miR-455-3p, among others. Comprehensive details about the regulatory connections between these miRNAs and their corresponding target genes are available in Table 8.

4 Discussion

Exogenous GAA administration modulates energy distribution within muscle cells (28, 29), leading to decreased activity of key metabolic enzymes and, consequently, reduced hepatic fat

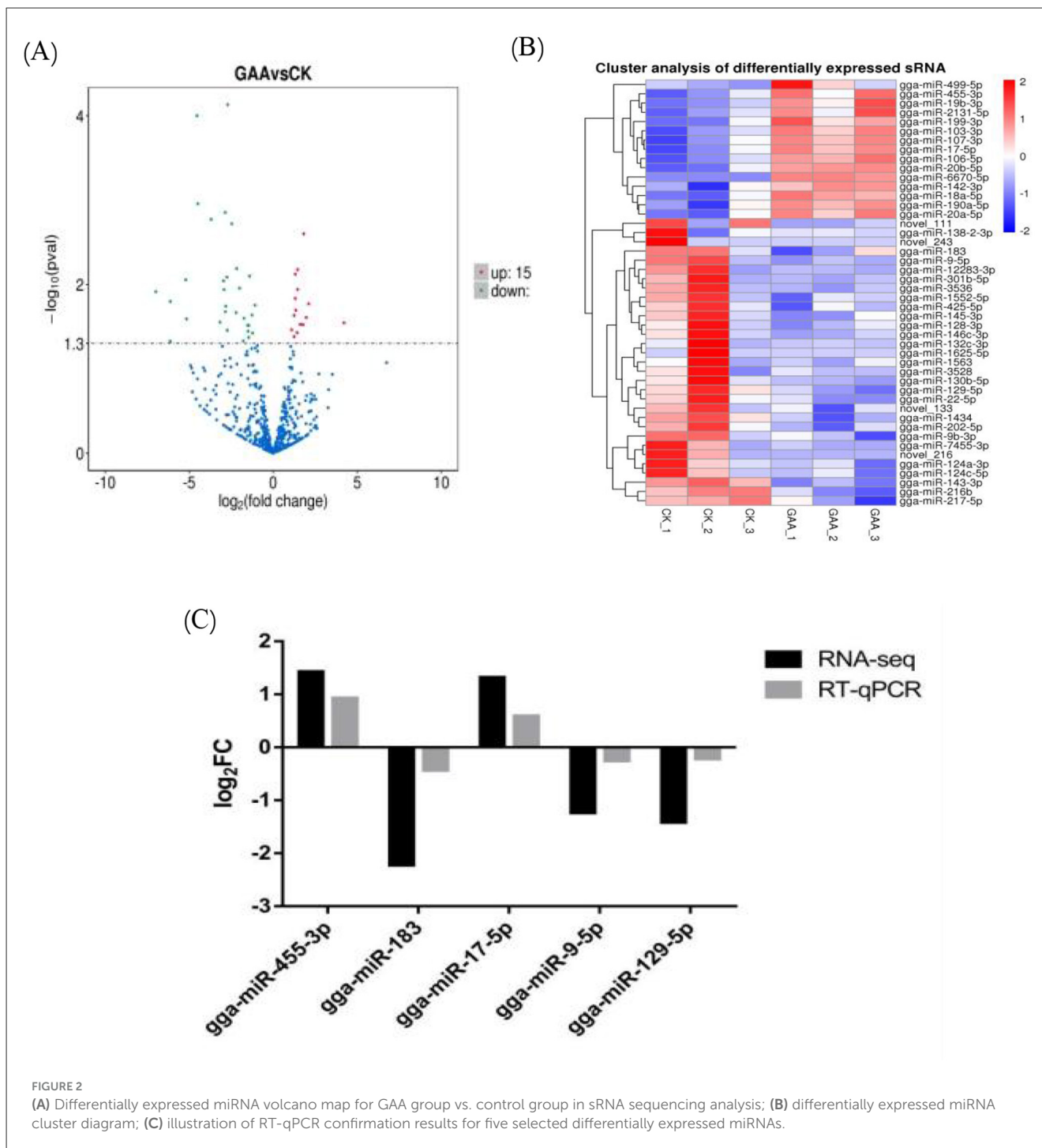


FIGURE 2 (A) Differentially expressed miRNA volcano map for GAA group vs. control group in sRNA sequencing analysis; (B) differentially expressed miRNA cluster diagram; (C) illustration of RT-qPCR confirmation results for five selected differentially expressed miRNAs.

synthesis. Additionally, it promotes the process of β -oxidation of fatty acids, ultimately contributing to a reduction in abdominal fat accumulation in broiler chickens (11, 30, 31). This occurs via either a reduction in adipocyte size or number. Our previous study revealed that a diet supplemented with 1,200 mg/kg of GAA reduced the abdominal fat content and size of adipocytes in broiler chicken. Therefore, we propose that GAA reduces fat storage by enhancing lipid metabolism and promoting the utilization of excess energy, thereby inhibiting its conversion into adipose tissue. To visually summarize the proposed molecular pathways

through which GAA may exert its anti-adipogenic effects, we have constructed a schematic model (refer to Figure 7).

To interpret these findings, we explored potential mechanistic insights from existing literature, primarily in mammalian models. TMEM is integral to muscle development and lipid metabolism. Research indicates a significant elevation in the overall level of diacylglycerol (DAG) in cells overexpressing TMEM68, demonstrating that DAG functions as an acyl receptor in the enzymatic reaction catalyzed by TMEM68 for triacylglycerol (TAG) formation, thereby highlighting TMEM8's role in regulating

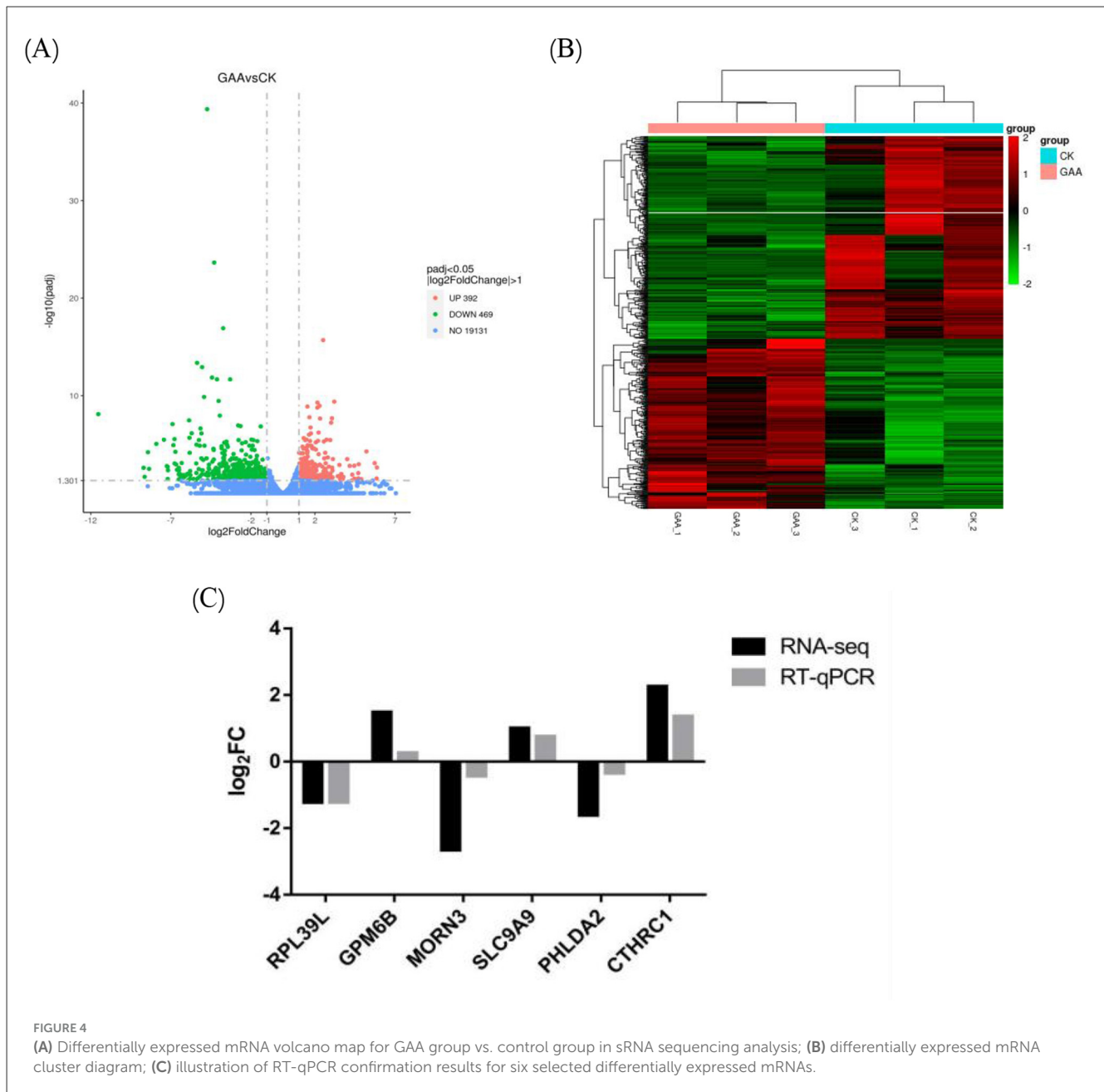


FIGURE 4

(A) Differentially expressed mRNA volcano map for GAA group vs. control group in sRNA sequencing analysis; (B) differentially expressed mRNA cluster diagram; (C) illustration of RT-qPCR confirmation results for six selected differentially expressed mRNAs.

central nervous system. According to Renström et al. (37) and Wiemerslage et al. (38), this regulation influences obesity and is implicated in the metabolic regulation of triglycerides and other lipids in adipocytes and pre-adipocytes. Although the specific function of TMEM35B in avian lipid metabolism is not yet defined, its downregulation in our study and its targeting by miRNAs suggest a potential, yet hypothetical, role in the GAA-mediated reduction of fat deposition.

Stearoyl-CoA desaturase (SCD) is a crucial fatty acid metabolism enzyme. It introduces a double bond between the ninth and tenth carbon atoms of saturated fatty acids (SFA). The process happens specifically with palmitoyl-CoA (C16:0) and stearoyl-CoA (C18:0) generating monoenoic fatty acids (MEFAs) such as palmitoleic acid (C16:1) as well as oleic acid

(C18:1) (39–41). SCD actively participates in the regulation of lipid metabolism.

Lipids are essential molecules that are made and broken down by living things. Monounsaturated fatty acids (MUFA) are vital in the synthesis of complex lipids, including triglycerides (TG), phospholipids, and cholesterol esters. The synthesis of these complex lipids is crucial for maintaining the structural integrity of cellular membranes, storing lipids in fat cells, and regulating energy metabolism (42). Research indicates that SCD plays a significant role in the metabolic pathway of fatty acids and is an essential element in the metabolism of unsaturated fatty acids (43). SCD is responsible for controlling the synthesis of monounsaturated fatty acids, which subsequently influences the fluidity of membranes and the metabolism of lipids within cells (39, 44, 45).

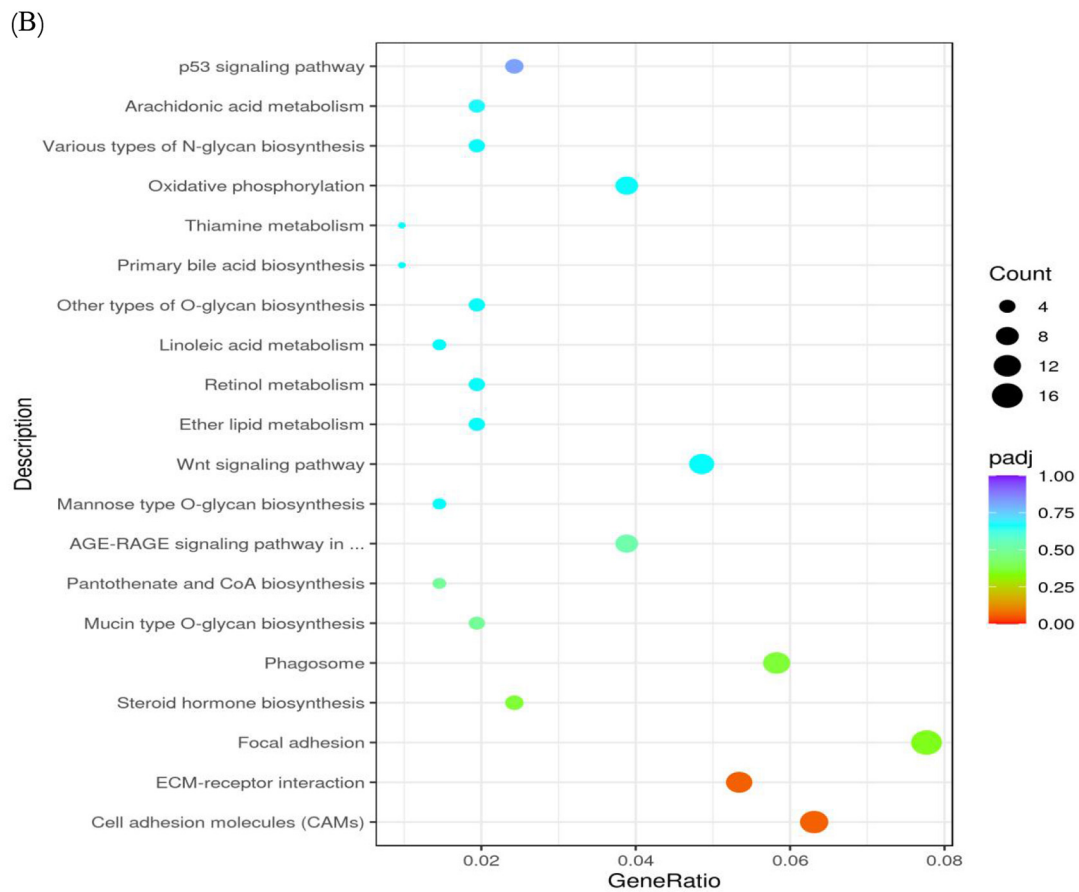
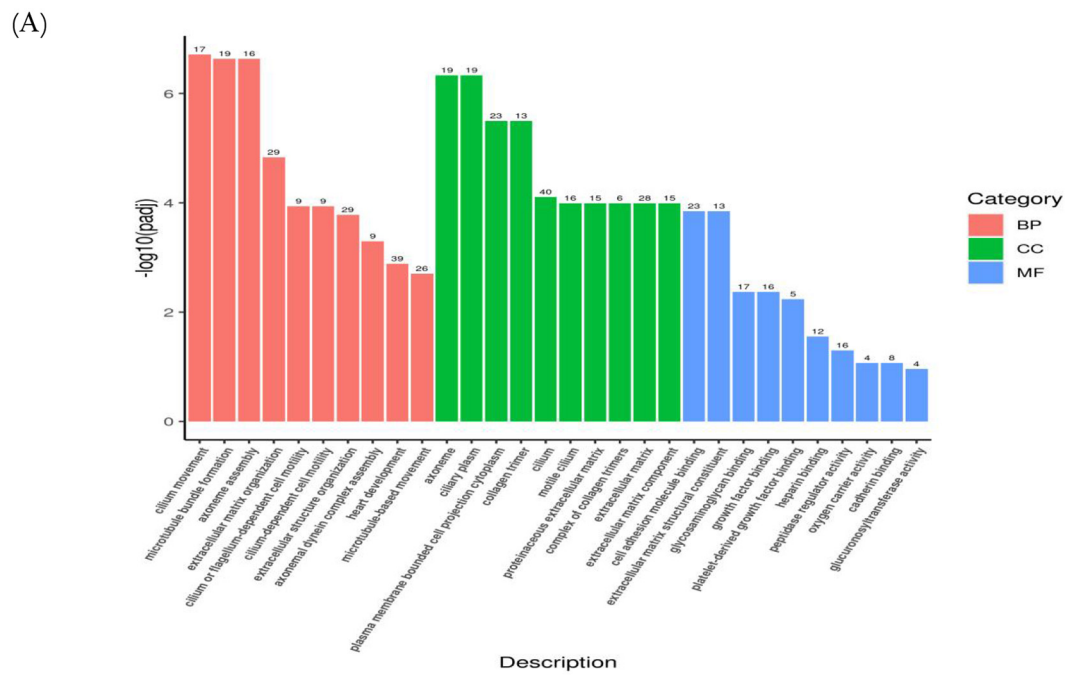
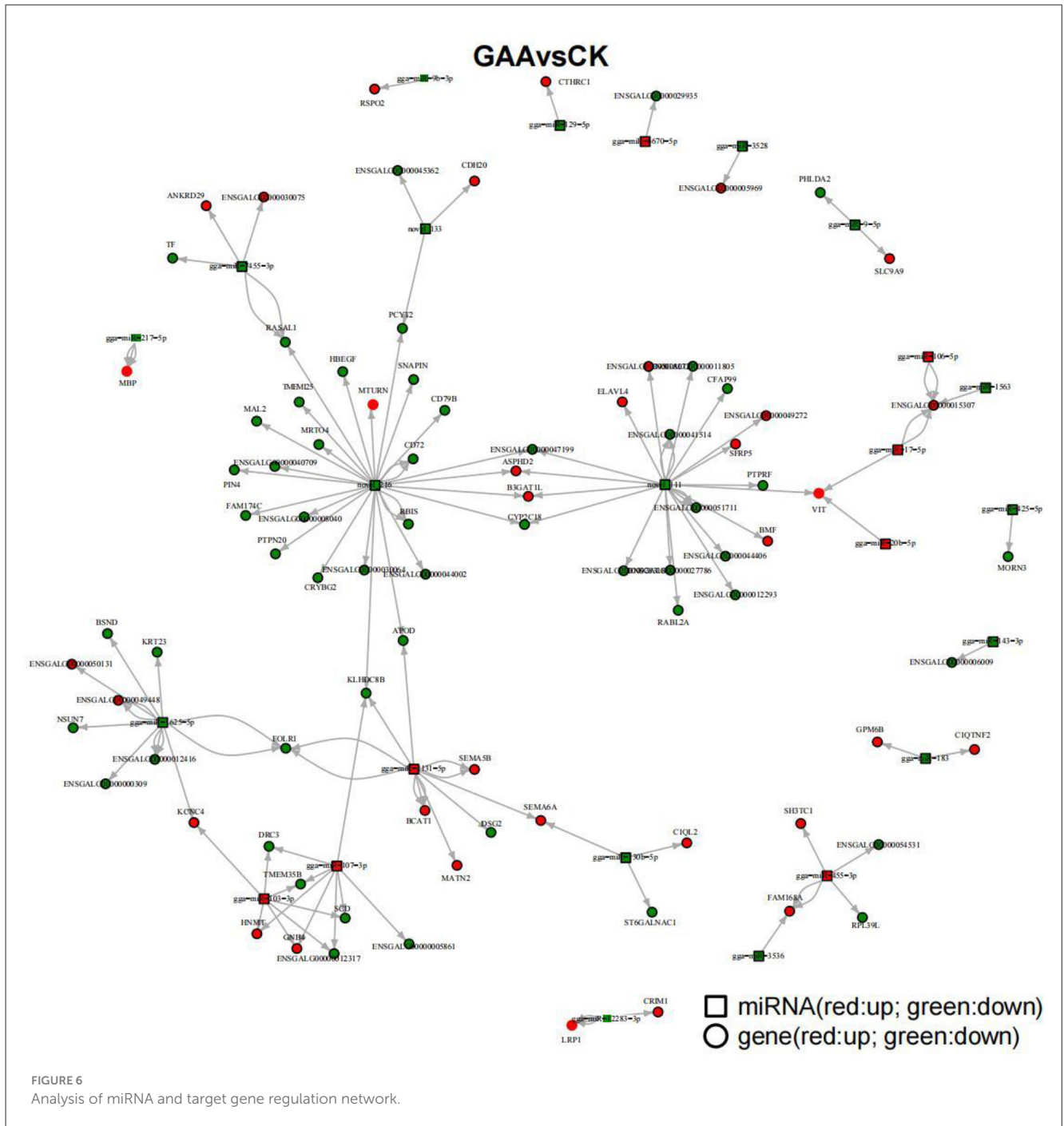


FIGURE 5
GO enrichment column (A) and KEGG enrichment scatter plot (B) of differentially expressed mRNA.



Studies with knockout mice and the model organism *Caenorhabditis elegans* show that SCD1 knockout (or deficiency) increases SFA and decreases MUFA and shifts fatty acid metabolism from biosynthesis to oxidation (19, 46). Mice that completely lack SCD1, known as global knockout (GKO) mice, show an elevated metabolic rate due to increased lipid oxidation, decreased lipid synthesis, and increased insulin sensitivity. These factors together confer resistance to obesity and fatty liver degeneration that often accompanies high-carbohydrate and high-fat diets in these mice (19). In high-fat diet-fed mice, the SCD1 inhibitor E6446 ameliorates hepatic steatosis, lipid droplet accumulation,

and insulin resistance by modulating hepatic lipid metabolism pathways (47). Therefore, the observed downregulation of SCD1 in our study aligns with a metabolic state that favors reduced lipid synthesis and/or increased oxidation, as seen in other models. However, its direct causal role in the context of GAA action in broilers remains to be functionally validated.

miRNAs are critical mediators of lipid synthesis, fat oxidation and lipoprotein production (48, 49). Among these, miR-103 is particularly notable for its significant role in insulin resistance and lipid metabolism. This specific microRNA inhibits *de novo* lipogenesis by targeting the fatty acid synthase gene (FASN) and

TABLE 8 Some miRNA and target gene regulation relationship.

miRNA	Target gene
gga-miR-9b-3p ↓	Up: RSPO2
gga-miR-129-5p ↓	Down: CTHRC1
gga-miR-7455-3p ↓	Up: ANKRD29
	Down: TF, RASAL1
gga-miR-217-5p ↓	Up: MBP
gga-miR-9-5p ↓	Up: SLC9A9
	Down: PHLDA2
gga-miR-17-5p ↑	Up: VIT
gga-miR-20b-5p ↑	Up: VIT
gga-miR-425-5p ↓	Down: MORN3
gga-miR-183 ↓	Up: GPM6B, C1QTNF2
gga-miR-1625-5p ↓	Up: KCNC4
	Down: BSND, KRT23, NSUN7, FOLR1
gga-miR-103-3p ↑	Up: KCNC4, HNMT, GNB4
	Down: DRC3, TMEM35B, SCD
gga-miR-107-3p ↑	Down: DRC3, TMEM35B, SCD, KLHDC8B
gga-miR-2131-5p ↑	Up: SEMA5B, SEMA6A, MATN2, BCAT1
	Down: DSG2, FOLR1, KLHDC8B, APOD
gga-miR-130b-5p ↓	Up: SEMA6A, C1QL2
	Down: ST6GALNAC1
gga-miR-12283-3p ↓	Up: CRIM1, LRP1
gga-miR-3536 ↓	Up: FAM168A
gga-miR-455-3p ↑	Up: SH3TC1, FAM168A
	Down: RPL39L

“↑↓” indicates the upregulation or downregulation of miRNA; up indicates the upregulation of target gene, and down indicates the downregulation of target gene.

SCD1 in murine liver tissues, thereby contributing to the mitigation of obesity and diet-induced fatty liver disease, as reported by Zhang et al. (50). In contrast, Holik et al. (51) in models utilizing 3T3-L1 mouse pre-adipocytes, it has been noted that miR-103 exerts a unique function by encouraging lipid accumulation. In 3T3-L1 mouse embryonic fibroblasts, miR-103-3p promotes adipocyte differentiation and lipid synthesis by inhibiting the myocyte enhancer factor 2D (MEF2D) and activating the protein kinase-B/mechanistic target of rapamycin (AKT/mTOR) signaling pathway (52, 53). When miR-103/107 is deactivated in adipocytes, noticeable changes occur, including reduced adipocyte size, decreased overall fat mass in mice, improved insulin sensitivity, and enhanced glucose uptake following insulin exposure, as indicated by Trajkovski et al. (21). During porcine adipocyte differentiation, the expression of miR-103-3p (an important subtype of miR-103) is significantly upregulated, while inhibiting its expression can effectively block the differentiation of preadipocytes (54). Additionally, Liu's study reveals that miR-103-3p plays a role in controlling the growth and lipid metabolism in epithelial cells

found within bovine mammary tissue (55). Lin and associates showed that a significant rise in pre-miR-103-1 expression in GMECs, attained through adenoviral infection, markedly increases triglyceride levels and lipid droplet formation in these cells (56). Our data indicate that the upregulation of miR-103-3p is associated with the downregulation of the SCD and TMEM35B genes. However, the role of miR-103-3p as a negative regulator of SCD and TMEM35B in broiler adipocytes necessitates further experimental validation.

MiR-107 plays essential roles in a spectrum of biological processes, including the regulation of insulin sensitivity, lipid metabolism, lipogenesis, tumor angiogenesis, and cell proliferation (21, 53, 57). Importantly, miR-107 influences the rise in lipid accumulation within the liver by impacting fatty acid oxidation, as evidenced by Bhatia et al. (58, 59). Furthermore, Ahonen et al. (60) demonstrated that miR-107 promotes adipocyte differentiation and ectopic fat accumulation by interacting with cyclin-dependent kinase 6 (CDK6). Research in bovine adipose tissue has demonstrated that miR-107, which is highly expressed there, inhibits adipocyte differentiation by modulating apolipoprotein C2 (APOC2) (61). It suggests that miR-103/107 induce pre-adipocyte apoptosis specifically through endoplasmic reticulum mechanisms and by stimulating the Wnt3a/ β -catenin pathway, pointing to a novel potential strategy against obesity and metabolic syndrome (62). Previous research has also identified miR-107 as a possible regulatory factor associated with abdominal fat accumulating in chickens (63). The expression of gga-miR-107-3p is negatively correlated with the levels of SCD and TMEM35B. This correlation suggests that miR-107-3p may exert the effect of GAA by suppressing SCD and TMEM35B in chicken, however, this regulatory relationship requires further verification through *in vitro* experiments in broilers.

5 Conclusion

This study demonstrates that dietary GAA effectively reduces abdominal fat deposition in broilers. Integrated omics analysis revealed a potential mechanism: GAA upregulates gga-miR-103-3p and gga-miR-107-3p, leading to the downregulation of key target genes, SCD and TMEM35B. Given the established role of SCD in lipogenesis and the putative role of TMEM proteins in lipid metabolism, this miR-103/107–SCD/TMEM35B axis provides a novel mechanistic explanation for the anti-adipogenic effect of GAA. Although this study has the above new findings, it still has the following limitations, including the sample size (three biological replicates per group) and the correlative nature of the omics data; thus, the proposed regulatory pathway requires further direct functional validation in avian models. Collectively, our work identifies a possible molecular pathway and provides a strong theoretical foundation for using GAA as a feed additive. These results suggest that GAA supplementation could be a viable strategy to enhance lean meat yield and improve carcass quality in commercial broiler production, potentially offering economic benefits through improved feed efficiency and product value.

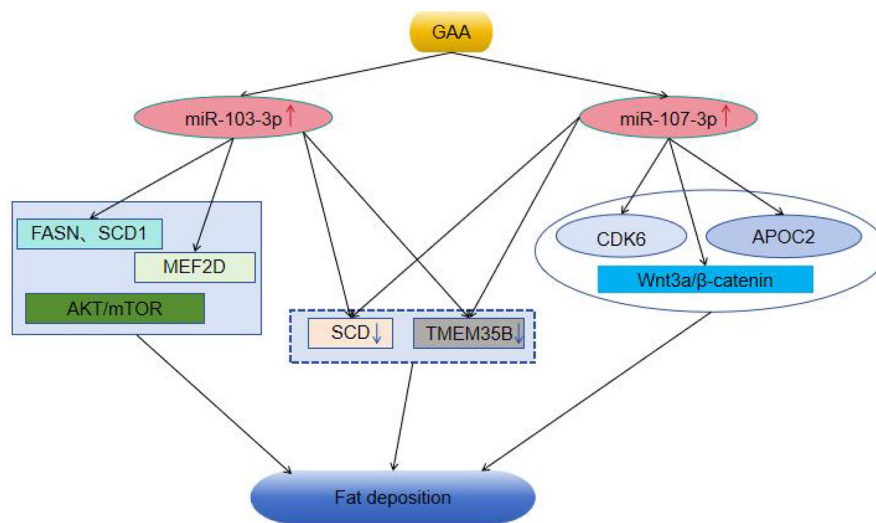


FIGURE 7

The mechanism by which GAA reduces fat deposition through miRNA-targeted gene regulatory signaling pathway. Note “↑↓” indicates upregulation or downregulation; an upward arrow denotes upregulation of the target gene, while a downward arrow denotes downregulation of the target gene.

Data availability statement

The raw data of transcriptome presented in the study are deposited in the Sequence Read Archive repository, accession number PRJNA1381682. The raw data of Small RNA transcriptome presented in the study are deposited in the Sequence Read Archive repository, accession number PRJNA1382004.

Ethics statement

The animal study was approved by the Life Sciences Ethics Committee at Yunnan Agricultural University (Approval ID: 202203094). The study was conducted in accordance with the local legislation and institutional requirements.

Author contributions

MLiu: Data curation, Formal analysis, Software, Visualization, Writing – original draft. JR: Data curation, Software, Writing – review & editing. YY: Data curation, Investigation, Methodology, Writing – original draft. MLi: Investigation, Methodology, Writing – review & editing. ZG: Investigation, Methodology, Writing – review & editing. CG: Conceptualization, Project administration, Resources, Writing – original draft. WC: Data curation, Funding acquisition, Investigation, Project administration, Validation, Writing – original draft.

Funding

The author(s) declared that financial support was received for this work and/or its publication. This research was funded by the National Natural Science Foundation of China (grant

No. 32202666); Yunnan Province Basic Research Special Project (202301AT070504); Yunnan Province Agricultural Joint Special Project (202301BD070001-108), and the Postdoctoral Orientation training program of Yunnan Province, China.

Acknowledgments

The authors would like to thank all the research assistants and laboratory technicians who contributed to the study. Furthermore, the authors wish to acknowledge the reviewers for their valuable comments and improvements to the manuscript.

Conflict of interest

The author(s) declared that this work was conducted in the absence of any commercial or financial relationships that could be construed as a potential conflict of interest.

Generative AI statement

The author(s) declared that generative AI was not used in the creation of this manuscript.

Any alternative text (alt text) provided alongside figures in this article has been generated by Frontiers with the support of artificial intelligence and reasonable efforts have been made to ensure accuracy, including review by the authors wherever possible. If you identify any issues, please contact us.

Publisher's note

All claims expressed in this article are solely those of the authors and do not necessarily represent those of their affiliated

organizations, or those of the publisher, the editors and the reviewers. Any product that may be evaluated in this article, or

claim that may be made by its manufacturer, is not guaranteed or endorsed by the publisher.

References

- Ma X, Sun J, Zhu S, Du Z, Li D, Li W, et al. MiRNAs and mRNAs analysis during abdominal preadipocyte differentiation in chickens. *Animals (Basel)*. (2020) 10:468. doi: 10.3390/ani10030468
- Tian W, Zhang B, Zhong H, Nie R, Ling Y, Zhang H, et al. Dynamic expression and regulatory network of circular RNA for abdominal preadipocytes differentiation in chicken (*Gallus gallus*). *Front Cell Dev Biol*. (2021) 9:761638. doi: 10.3389/fcell.2021.761638
- Nematbakhsh S, Pei Pei C, Selamat J, Nordin N, Idris LH, Abdull Razis AF. Molecular regulation of lipogenesis, adipogenesis and fat deposition in chicken. *Genes (Basel)*. (2021) 12:414. doi: 10.3390/genes12030414
- Chen Y, Akhtar M, Ma Z, Hu T, Liu Q, Pan H, et al. Chicken cecal microbiota reduces abdominal fat deposition by regulating fat metabolism. *NPJ Biofilms Microbiomes*. (2023) 9:28. doi: 10.1038/s41522-023-00390-8
- Peña-Saldrriaga LM, Fernández-López J, Pérez-Alvarez JA. Quality of chicken fat by-products: lipid profile and colour properties. *Foods*. (2020) 9:1046. doi: 10.3390/foods9081046
- Wan X, Yang Z, Ji H, Li N, Yang Z, Xu L, et al. Effects of lycopene on abdominal fat deposition, serum lipids levels and hepatic lipid metabolism-related enzymes in broiler chickens. *Anim Biosci*. (2021) 34:385–92. doi: 10.5713/ajas.20.0432
- Chen Y, Zhao Y, Jin W, Li Y, Zhang Y, Ma X, et al. MicroRNAs and their regulatory networks in Chinese Gushi chicken abdominal adipose tissue during postnatal late development. *BMC Genomics*. (2019) 20:778. doi: 10.1186/s12864-019-6094-2
- Luo N, Shu J, Yuan X, Jin Y, Cui H, Zhao G, et al. Differential regulation of intramuscular fat and abdominal fat deposition in chickens. *BMC Genomics*. (2022) 23:308. doi: 10.1186/s12864-022-08538-0
- Ostojic SM. Advanced physiological roles of guanidinoacetic acid. *Eur J Nutr*. (2015) 54:1211–5. doi: 10.1007/s00394-015-1050-7
- Portocarero N, Braun U. The physiological role of guanidinoacetic acid and its relationship with arginine in broiler chickens. *Poult Sci*. (2021) 100:101203. doi: 10.1016/j.psj.2021.101203
- Michiels J, Maertens L, Buyse J, Lemme A, Rademacher M, Dierick NA, et al. Supplementation of guanidinoacetic acid to broiler diets: effects on performance, carcass characteristics, meat quality, and energy metabolism. *Poult Sci*. (2012) 91:402–12. doi: 10.3382/ps.2011-01585
- Yazdi TF, Golian A, Zarghi H, Mehdi V. Effect of wheat-soy diet nutrient density and guanidine acetic acid supplementation on performance and energy metabolism in broiler chickens. *Ital J Anim Sci*. (2017) 16:593–600. doi: 10.1080/1828051X.2017.1305260
- Zhang S, Zang C, Pan J, Ma C, Wang C, Li X, et al. Effects of dietary guanidinoacetic acid on growth performance, guanidinoacetic acid absorption and creatine metabolism of lambs. *PLoS ONE*. (2022) 17:e0264864. doi: 10.1371/journal.pone.0264864
- Mousavi S, Afsar A, Lotfollahian H. Effects of guanidinoacetic acid supplementation to broiler diets with varying energy contents. *J Appl Poult Res*. (2013) 22:47–54. doi: 10.3382/japr.2012-00575
- DeGroot AA, Braun U, Dilger RN. Guanidinoacetic acid is efficacious in improving growth performance and muscle energy homeostasis in broiler chicks fed arginine-deficient or arginine-adequate diets. *Poult Sci*. (2019) 98:2896–905. doi: 10.3382/ps/pez036
- Majdiddin M, Braun U, Lemme A, Golian A, Kermanshahi H, De Smet S, et al. Guanidinoacetic acid supplementation improves feed conversion in broilers subjected to heat stress associated with muscle creatine loading and arginine sparing. *Poult Sci*. (2020) 99:4442–53. doi: 10.1016/j.psj.2020.05.023
- Guimarães-Ferreira L. Role of the phosphocreatine system on energetic homeostasis in skeletal and cardiac muscles. *Einstein (São Paulo)*. (2014) 12:126–31. doi: 10.1590/S1679-45082014RB2741
- Lee N, Kim I, Park S, Han D, Ha S, Kwon M, et al. Creatine inhibits adipogenesis by downregulating insulin-induced activation of the phosphatidylinositol 3-kinase signaling pathway. *Stem Cells Dev*. (2015) 24:983–94. doi: 10.1089/scd.2014.0130
- Ntambi JM, Miyazaki M, Stoehr JP, Lan H, Kendziora CM, Yandell BS, et al. Loss of stearoyl-CoA desaturase-1 function protects mice against adiposity. *Proc Natl Acad Sci U S A*. (2002) 99:11482–6. doi: 10.1073/pnas.132384699
- Brown JM, Rudel LL. Stearoyl-coenzyme A desaturase 1 inhibition and the metabolic syndrome: considerations for future drug discovery. *Curr Opin Lipidol*. (2010) 21:192–7. doi: 10.1097/MOL.0b013e32833854ac
- Trajkovski M, Hausser J, Soutschek J, Bhat B, Akin A, Zavolan M, et al. MicroRNAs 103 and 107 regulate insulin sensitivity. *Nature*. (2011) 474:649–53. doi: 10.1038/nature10112
- Li S, Wang C, Wu Z, Liu Q, Guo G, Huo W, et al. Effects of guanidinoacetic acid supplementation on growth performance, nutrient digestion, rumen fermentation and blood metabolites in Angus bulls. *Animal*. (2020) 14:2535–42. doi: 10.1017/S1751731120001603
- Wu H, Xie J, Peng W, Ji F, Qian J, Shen Q, et al. Effects of guanidinoacetic acid supplementation on liver and breast muscle fat deposition, lipid levels, and lipid metabolism-related gene expression in ducks. *Front Vet Sci*. (2024) 11:1364815. doi: 10.3389/fvets.2024.1364815
- Rahmawati D, Hanim C, Annas M, Sasongko H, Ariyadi B. Effect of guanidinoacetic acid in feed with different protein levels on the performance and internal organ characteristics of broiler chickens. In: *Proceedings of the 3rd International Conference on Smart and Innovative Agriculture (ICoSIA 2022)* (2023). doi: 10.2991/978-94-6463-122-7_30
- Yan Z, Yan Z, Liu S, Yin Y, Yang T, Chen Q. Regulatory mechanism of guanidinoacetic acid on skeletal muscle development and its application prospects in animal husbandry: a review. *Front Nutr*. (2021) 8:714567. doi: 10.3389/fnut.2021.714567
- Heydar Z, Abolghasem G, Forouzan YT. Effect of dietary sulphur amino acid levels and guanidinoacetic acid supplementation on performance, carcass yield and energetic molecular metabolites in broiler chickens fed wheat-soy diets. *Ital J Anim Sci*. (2020) 19:951–59. doi: 10.1080/1828051X.2020.1809537
- Hong J, Raza SHA, Liu M, Li M, Ruan J, Jia J, et al. Association analysis of transcriptome and quasi-targeted metabolomics reveals the regulation mechanism underlying broiler muscle tissue development at different levels of dietary guanidinoacetic acid. *Front Vet Sci*. (2024) 11:1384028. doi: 10.3389/fvets.2024.1384028
- Majdiddin M, Braun U, Lemme A, Golian A, Kermanshahi H, De Smet S, et al. Effects of feeding guanidinoacetic acid on oxidative status and creatine metabolism in broilers subjected to chronic cyclic heat stress in the finisher phase. *Poult Sci*. (2023) 102:102653. doi: 10.1016/j.psj.2023.102653
- Janes D Jr, Suehs B, Gatlin DM 3rd. Dietary creatine and guanidinoacetic acid supplementation have limited effects on hybrid striped bass. *Fish Physiol Biochem*. (2023) 49:399–407. doi: 10.1007/s10695-023-01196-3
- Khalil S, Saenbungkhon N, Kesnava K, Sivapurinthep P, Siththiripong R, Jumanee S, et al. Effects of guanidinoacetic acid supplementation on productive performance, pectoral myopathies, and meat quality of broiler chickens. *Animals*. (2021) 11:3180. doi: 10.3390/ani1113180
- Asiriwardhana M, Bertolo RF. Guanidinoacetic acid supplementation: a narrative review of its metabolism and effects in swine and poultry. *Front Anim Sci*. (2022) 3:972868. doi: 10.3389/fanim.2022.972868
- Wang Y, Zeng F, Zhao Z, He L, He X, Pang H, et al. Transmembrane protein 68 functions as an MGAT and DGAT enzyme for triacylglycerol biosynthesis. *Int J Mol Sci*. (2023) 24:2012. doi: 10.3390/ijms24032012
- McLelland GL, Lopez-Osias M, Verzijl CRC, Ellenbroek BD, Oliveira RA, Boon NJ, et al. Identification of an alternative triglyceride biosynthesis pathway. *Nature*. (2023) 621:171–8. doi: 10.1038/s41586-023-06497-4
- Zhou H, Zhu X, Yao Y, Su Y, Xie J, Zhu M, et al. TMEM88 modulates lipid synthesis and metabolism cytokine by regulating Wnt/ β -catenin signaling pathway in non-alcoholic fatty liver disease. *Front Pharmacol*. (2022) 12:798735. doi: 10.3389/fphar.2021.798735
- Li L, Yang C, Li S, Liu Y, Li H, Hu S, et al. TMEM88 modulates the secretion of inflammatory factors by regulating YAP signaling pathway in alcoholic liver disease. *Inflamm Res*. (2020) 69:789–800. doi: 10.1007/s00011-020-01360-y
- Tang J, Song H, Li S, Lam SM, Ping J, Yang M, et al. TMEM16F expressed in Kupffer cells regulates liver inflammation and metabolism to protect against listeria monocytogenes. *Adv Sci (Weinh)*. (2024) 11:e2402693. doi: 10.1002/adv.202402693
- Renström F, Payne F, Nordström A, Brito EC, Rolandsson O, Hallmans G, et al. Replication and extension of genome-wide association study results for obesity in 4923 adults from northern Sweden. *Hum Mol Genet*. (2009) 18:1489–96. doi: 10.1093/hmg/ddp041
- Wiemerslage L, Gohel PA, Maestri G, Hilmarsen TG, Mickael M, Fredriksson R, et al. The Drosophila ortholog of TMEM18 regulates insulin and glucagon-like signaling. *J Endocrinol*. (2016) 229:233–43. doi: 10.1530/JOE-16-0040

39. Dobrzyn A, Ntambi JM. The role of stearoyl-CoA desaturase in the control of metabolism. *Prostaglandins Leukot Essent Fatty Acids*. (2005) 73:35–41. doi: 10.1016/j.plefa.2005.04.011
40. Zhang H, Dong X, Wang Z, Zhou A, Peng Q, Zou H, et al. Dietary conjugated linoleic acids increase intramuscular fat deposition and decrease subcutaneous fat deposition in Yellow Breed × Simmental cattle. *Anim Sci J*. (2016) 87:517–24. doi: 10.1111/asj.12447
41. Jiang Z, Michal JJ, Tobey DJ, Daniels TF, Rule DC, Macneil MD. Significant associations of stearoyl-CoA desaturase (SCD1) gene with fat deposition and composition in skeletal muscle. *Int J Biol Sci*. (2008) 4:345–51. doi: 10.7150/ijbs.4.345
42. Sampath H, Ntambi JM. Role of stearoyl-CoA desaturase-1 in skin integrity and whole body energy balance. *J Biol Chem*. (2014) 289:2482–8. doi: 10.1074/jbc.R113.516716
43. Gunawan A, Listyarni K, Furqon A, Jakaria, Sumantri C, Akter SH, et al. RNA deep sequencing reveals novel transcripts and pathways involved in the unsaturated fatty acid metabolism in chicken. *Gene Rep*. (2019) 15:100370. doi: 10.1016/j.genrep.2019.100370
44. Hardy S, Langelier Y, Prentki M. Oleate activates phosphatidylinositol 3-kinase and promotes proliferation and reduces apoptosis of MDA-MB-231 breast cancer cells, whereas palmitate has opposite effects. *Cancer Res*. (2000) 60:6353–8.
45. Castro LF, Wilson JM, Gonçalves O, Galante-Oliveira S, Rocha E, Cunha I. The evolutionary history of the stearoyl-CoA desaturase gene family in vertebrates. *BMC Evol Biol*. (2011) 11:132. doi: 10.1186/1471-2148-11-132
46. Igal RA. Stearoyl-CoA desaturase-1: a novel key player in the mechanisms of cell proliferation, programmed cell death and transformation to cancer. *Carcinogenesis*. (2010) 31:1509–15. doi: 10.1093/carcin/bgq131
47. Wang W, Kong Y, Wang X, Wang Z, Tang C, Li J, et al. Identification of novel SCD1 inhibitor alleviates nonalcoholic fatty liver disease: critical role of liver-adipose axis. *Cell Commun Signal*. (2023) 21:268. doi: 10.1186/s12964-023-01297-9
48. Tsai WC, Hsu SD, Hsu CS, Lai TC, Chen SJ, Shen R, et al. MicroRNA-122 plays a critical role in liver homeostasis and hepatocarcinogenesis. *J Clin Invest*. (2012) 122:2884–97. doi: 10.1172/JCI63455
49. Zheng T, Chen H. Resveratrol ameliorates the glucose uptake and lipid metabolism in gestational diabetes mellitus mice and insulin-resistant adipocytes via miR-23a-3p/NOV axis. *Mol Immunol*. (2021) 137:163–73. doi: 10.1016/j.molimm.2021.06.011
50. Zhang M, Tang Y, Tang E, Lu W. MicroRNA-103 represses hepatic *de novo* lipogenesis and alleviates NAFLD via targeting FASN and SCD1. *Biochem Biophys Res Commun*. (2020) 524:716–22. doi: 10.1016/j.bbrc.2020.01.143
51. Holik AK, Lieder B, Kretschy N, Somoza MM, Held S, Somoza V. N(ε)-Carboxymethyllysine increases the expression of miR-103/143 and enhances lipid accumulation in 3T3-L1 cells. *J Cell Biochem*. (2016) 117:2413–22. doi: 10.1002/jcb.25576
52. Chen L, Dai Y, Ji C, Yang L, Shi C, Xu G, et al. MiR-146b is a regulator of human visceral preadipocyte proliferation and differentiation and its expression is altered in human obesity. *Mol Cell Endocrinol*. (2014) 393:65–74. doi: 10.1016/j.mce.2014.05.022
53. Li M, Liu Z, Zhang Z, Liu G, Sun S, Sun C. miR-103 promotes 3T3-L1 cell adipogenesis through AKT/mTOR signal pathway with its target being MEF2D. *Biol Chem*. (2015) 396:235–44. doi: 10.1515/hsz-2014-0241
54. Li G, Wu Z, Li X, Ning X, Li Y, Yang G. Biological role of microRNA-103 based on expression profile and target genes analysis in pigs. *Mol Biol Rep*. (2011) 38:4777–86. doi: 10.1007/s11033-010-0615-z
55. Liu X, Sun B, Zhang F, Zhong Z, Zhang Y, Li F, et al. lncRNA MPFAST promotes proliferation and fatty acid synthesis of bovine mammary epithelial cell by sponging miR-103 regulating PI3K-AKT pathway. *J Agric Food Chem*. (2022) 70:12004–13. doi: 10.1021/acs.jafc.2c04789
56. Lin X, Luo J, Zhang L, Wang W, Gou D. MiR-103 controls milk fat accumulation in goat (*Capra hircus*) mammary gland during lactation. *PLoS ONE*. (2013) 8:e79258. doi: 10.1371/journal.pone.0079258
57. Hennessy EJ, Sheedy FJ, Santamaria D, Barbadic M, O'Neill LA. Toll-like receptor-4 (TLR4) down-regulates microRNA-107, increasing macrophage adhesion via cyclin-dependent kinase 6. *J Biol Chem*. (2011) 286:25531–9. doi: 10.1074/jbc.M111.256206
58. Bhatia H, Pattnaik BR, Datta M. Inhibition of mitochondrial β -oxidation by miR-107 promotes hepatic lipid accumulation and impairs glucose tolerance *in vivo*. *Int J Obes (Lond)*. (2016) 40:861–9. doi: 10.1038/ijo.2015.225
59. Bhatia H, Verma G, Datta M. miR-107 orchestrates ER stress induction and lipid accumulation by post-transcriptional regulation of fatty acid synthase in hepatocytes. *Biochim Biophys Acta*. (2014) 1839:334–43. doi: 10.1016/j.bbarm.2014.02.009
60. Ahonen MA, Haridas PAN, Mysore R, Wabitsch M, Fischer-Posovszky P, Olkkonen VM. miR-107 inhibits CDK6 expression, differentiation, and lipid storage in human adipocytes. *Mol Cell Endocrinol*. (2019) 479:110–6. doi: 10.1016/j.mce.2018.09.007
61. Wei X, Zhao X, Shan X, Zhu Y, Wang S, Chen H, et al. MiR-107 regulates adipocyte differentiation and adipogenesis by targeting apolipoprotein C-2 (APOC2) in Bovine. *Genes (Basel)*. (2022) 13:1467. doi: 10.3390/genes13081467
62. Zhang Z, Wu S, Muhammad S, Ren Q, Sun C. miR-103/107 promote ER stress-mediated apoptosis via targeting the Wnt3a/ β -catenin/ATF6 pathway in preadipocytes. *J Lipid Res*. (2018) 59:843–53. doi: 10.1194/jlr.M082602
63. Liu Z, Cheng S, Zhang X, Yang M, Wei J, Ye F, et al. Characterization of the regulatory network and pathways in duodenum affecting chicken abdominal fat deposition. *Poult Sci*. (2024) 103:104463. doi: 10.1016/j.psj.2024.104463